Talanta 104 (2013) 32–38

Contents lists available at SciVerse ScienceDirect

Talanta

journal homepage: www.elsevier.com/locate/talanta

Quenching effect on gold nano-patterned cardiac troponin I chip by total internal reflection fluorescence microscopy

Seungah Lee, Seong Ho Kang*

Department of Applied Chemistry, College of Applied Science, Kyung Hee University, Yongin-si, Gyeonggi-do 446-701, Republic of Korea

ARTICLE INFO

Article history:
Received 23 September 2012
Received in revised form
7 November 2012
Accepted 8 November 2012
Available online 17 November 2012

Keywords:
Cardiac troponin I (cTnI)
Nanoarray protein chip
High-sensitivity
Total internal reflection fluorescence microscopy (TIRFM)

ABSTRACT

Total internal reflection fluorescence microscopy (TIRFM) was investigated for enhanced detection sensitivity of cardiac troponin I (cTnI) on a gold nano-patterned protein chip. A 4×5 nanoarray patterning of a gold chip based on a single-molecule sandwich immunoassay was prepared with a spot diameter of 500 nm on glass substrates formed *via* electron-beam nanolithography. Quantitative trace analysis was possible as a function of increasing total internal reflection fluorescence intensity in the range of 84 aM–350 pM at prism-type and 35 aM–350 pM at objective-type TIRFM. Although using same gold nano-patterned cTnI chips, however, the objective-type TIRFM showed enhanced detection sensitivities 2.4 times better than the prism-type due to weaker gold quenching. This result is also about 7000 times lower in the detection limit compared with those obtained by conventional commercial sandwich enzyme-linked immunosorbent assay techniques.

1. Introduction

Total internal reflection fluorescence microscopy (TIRFM) has been one of the most common technique for the single-molecule study of cell–substrate surfaces or cell membranes in order to acqure detailed information about the behavior of biomolecules [1,2]. TIRFM systems are typically available in two configurations, prism- and objective-type. Prism-type TIRFM is useful to obtain high-quality images with high signal-to-noise ratios and has been used extensively to study molecular dynamics at liquid/solid interfaces [3,4]. More recently, it has been applied in nanoarray protein chips based on single-molecule sandwich immunoassay for clinical diagnosis [5]. The majority of designs are centered on upright microscopy with an added prism to direct laser illumination toward the interface where total internal reflection occurs, located in the specimen conjugate plane of the microscope. Subsequently, the reflected ray is removed from the specimen *via* the prism. Tokunaga et al. [6] have developed a different type of TIRFM, the objective-type TIRFM, which had free space above the coverglass. The advantage of objective-type TIRFM was the possibility of integration with scanning probe microscopy, as well as combination with other techniques utilized in cell biology, such as a micro-incubator [7,8]. In this technique, the laser beam was introduced into the periphery of the back aperture of the objective. By focusing the laser beam at the back focal plane of the objective, a parallel beam emerges from the objective lens. The angle at which the beam emerges from the objective depends on its entry position into the back focal plane. However, this technique is not suitable if the penetration depth of the evanescent wave requires adjustment because the objective-type TIRFM has been commercialized [9,10]. Therefore intensive researches based on quantitative analysis of fluorescence signals are necessary for experimental comparison of the structural property of current systems.

When located in close proximity to metals, a fluorescent dye exhibits strong changes in its electronic and optical properties, likely as a result of mixing the molecule and metal electronic levels, as well as interaction of the molecule with the surface plasmon resonance [11,12]. In particular, gold quenching of the dye emission occurred due to energy transfer [13], electron transfer [14], or decreasing the radiative rate of the dye [15]. This phenomenon was important for labeled antibodies used in immunoassays, where self-quenching of the fluorophore limits the brightness available per labeled protein [16]. Moreover, the highly sensitive optical immunosensor using surface enhanced Raman spectroscopy overcame its major drawback of reproducibility and was able to be used for quantitative analysis on a gold-patterned microarray chip [17]. However, a report addressing the quenching effect according to the configuration of a TIRFM system has not yet been directly supported by experimental evidence.

Here, both prism- and objective-type TIRFM configurations were used for ultra-sensitive immunoassay based on ultra-miniaturized arrays formed *via* a gold nano-patterned chip. As a model analyte, cardiac troponin I (cTnI), a specific biomarker of

* Corresponding author. Tel.: +82 31 201 3349; fax: +82 31 201 2340.
E-mail address: shkang@khu.ac.kr (S.H. Kang).

0039-9140/$ - see front matter © 2012 Elsevier B.V. All rights reserved.
http://dx.doi.org/10.1016/j.talanta.2012.11.014

acute myocardial infarction [18], was quantified by TIRF intensities corrected by background subtraction. The intensity varied depending on the optical configuration of the TIRFM due to quenching efficiency of gold nano-patterned on glass substrates.

2. Materials and methods

2.1. Reagents preparation

Dithiobis(succinimidyl propionate) (DSP) and Protein A/G were purchased from Pierce (Rockford, IL, USA). Dimethyl sulfoxide (DMSO), glycine, and Alexa Fluor® 647 donkey anti-mouse IgG were obtained from Sigma-Aldrich Inc. (St. Louis, MO, USA). Tris(base) was purchased from Mallinckrodt Baker, Inc. (Phillipsburg, NJ, USA). StabilGuard was purchased from Surmodics (Eden Prairie, MN, USA). Monoclonal mouse anti-cardiac troponin I antibody (clone 19C7 and 16A11) and standard human cardiac troponin I (cTnI, clone 8T53) were purchased from HyTest (Turku, Finland). Normal human serum samples were isolated from blood by centrifugation at 2000 rpm for 15 min at 2 °C. To mimic clinical conditions, serial dilution of the standard cTnI sample spiked into normal human serum was performed. Prior to use, 1 × PBS buffer solution (pH 7.4; 137 mM NaCl, 2.7 mM KCl, 4.3 mM Na_2HPO_4, 1.4 mM KH_2PO_4) was filtered through a 0.2 μm membrane filter and photobleached overnight using a UV-B lamp (G15TE, 280–315 nm, Philips, Netherlands).

2.2. Gold nano-patterned cTnI chip

The gold nano-patterned substrate was designed such as those shown in Fig. 1A and was subsequently fabricated by the National Nanofab Center (Daejeon, South Korea). A four inch soda–lime glass wafer was purchased from Winwin Tech (Bucheon, South Korea). A 4 × 5 nanoarray was fabricated to include 500 nm-diameter spots (Fig. 1B) with a 10 μm pitch, and the gold spots were deposited on a glass substrate by an electron beam evaporator (Fig. 1A). These substrates were coated with a 5 nm adhesive layer of chromium (99.997% purity) at a rate of 0.1 nm/s, followed by the deposition of a 20 nm layer of gold (99.997% purity) at a rate of 0.1 nm/s. Prior to linker deposition, the chips were immersed in acetone (99.5% purity) for 30 s and then isopropyl alcohol (99.9% purity) for 30 s. The gold nano-patterned biochips were exposed to piranha solution (1:1 = H_2SO_4:30% H_2O_2) for 30 min, rinsed with deionized water, and dried under a stream of nitrogen. Prior to use, the chips were stored in a desiccator.

2.3. cTnI sandwich immunoassay on gold nano-patterned chip

The sandwich immunoassay process of cTnI on gold substrate is shown in Fig. 1C. The gold patterned chip was immersed in 4 mg/mL DSP in DMSO for 30 min, then rinsed with DMSO and distilled water. 0.1 mg/mL Protein A/G in PBS was added to the activated-gold surface for 1 h. Unreacted succinimide groups were blocked by reacting with 10 mM Tris (pH 7.5) and 1 M glycine for 30 min. The chips were incubated with StabilGuard for 30 min to stabilize the bound proteins and then rinsed briefly with a few drops of distilled water. The chips were incubated with 20 μL of 2 μg/mL purified anti-human cTnI (19C7) in PBS pH 7.4 for 1 h. After washing, 20 μL cTnI standard protein (8T53) was diluted to various concentrations, including the normal or spiked clinical samples, and incubated on a biochip for 1 h. 20 μL of 2 μg/mL anti-human cTnI (16A11) was reacted for 1 h. Finally, 20 μL of 2 μg/mL Alexa Fluor® 647 donkey anti-mouse IgG reacted for 30 min to measure the TIRFM fluorescence intensity. The biochip was washed by dipping it in 100 mL 1 × PBS for 2 min at each step. All of the reactions were carried out at room temperature with agitation.

2.4. Both TIRFM systems

The physical layouts and schematic diagrams of the two TIRFM configurations are shown in Fig. 2. The TIRFM prism-type system (Fig. 2A), which was similar to a previously described design, was used to detect the antibody–antigen interactions on the gold nano-patterned protein array chips [5]. Briefly, the TIRFM was constructed

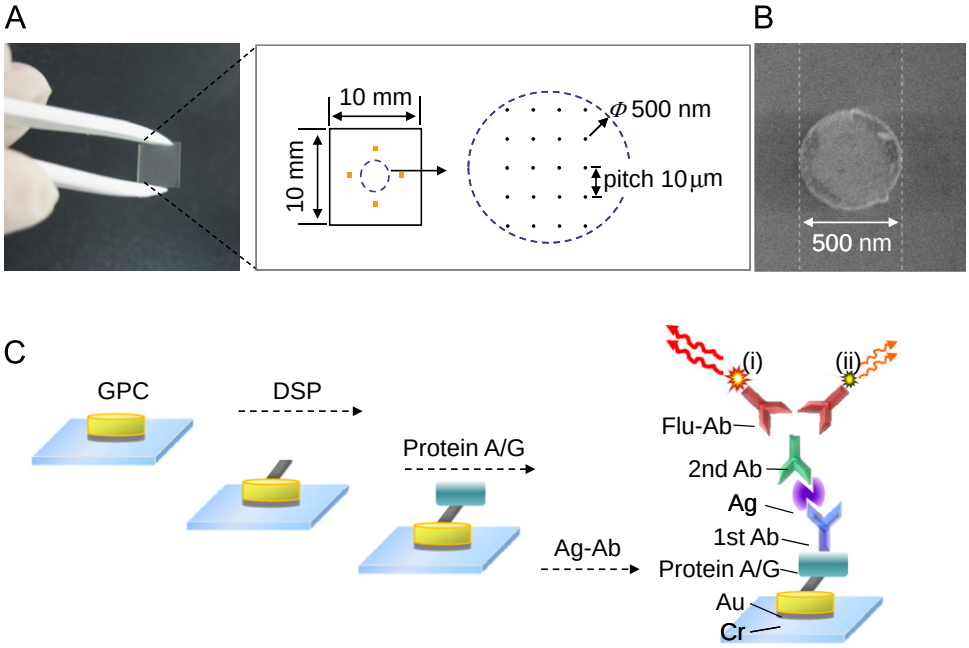

Fig. 1. (A) Design of the 4 × 5 nanoarray patterning of gold with a spot diameter of 500 nm on the glass substrate, (B) SEM image of an individual gold particle, and (C) schematic diagram of the sandwich fluorescence immunoassay on the gold nano-patterned protein chip. (i) and (ii) mean the fluorescence intensity using an objective-type TIRFM and prism-type TIRFM system. The chip was patterned with a 5 nm layer of chromium and a 20 nm layer of gold. The following acronyms are used: GPC, gold nano-patterned chip; DSP, dithiobis(succinimidyl propionate); Ag, antigen; Ab, antibody; Flu-Ab, Alexa Fluor® 647 donkey anti-mouse IgG.

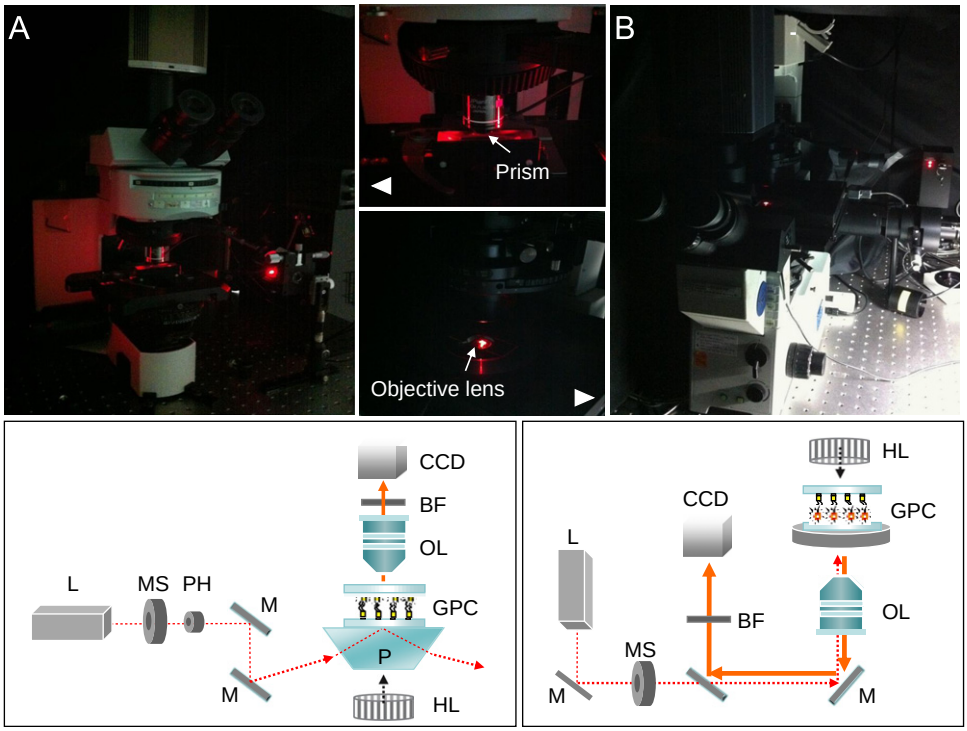

Fig. 2. Physical layouts of the (A) prism-type system and (B) objective-type system. Schematic diagrams of both TIRFM systems used for the quantitative analysis of cTnI (Bottom). The following acronyms are used: L, laser; MS, mechanical shutter; PH, pinhole; M, mirror; P, dove prism; GPC, gold nano-patterned chip; OL, objective lens; BF, band-pass filter; CCD, charge-coupled device; HL, halogen lamp.

using a transmitted all-side polished dove-type prism with anti-reflective coating (BK7, 15 mm × 63 mm × 15 mm, n=1.522, Korea Electro-Optics Co., Ltd., Korea). The TIRFM optics were incorporated into an upright Olympus BX51 microscope (Olympus Optical Co., Ltd., Shinjuku-ku, Tokyo, Japan) using an Olympus 100× UPlanFl (oil type, 1.3 N.A.) objective lens. A filter cube with a 680/30 nm band-pass filter (Semrock, Inc., NY, USA) was used to carry out the TIRFM study. An electron-multiplying cooled charge-coupled device (EM-CCD) camera (QuantEM 512SC, Photometrics, Tucson, AZ, USA) was mounted on the top of the microscope and was used with an exposure time of 100 ms.

In objective-type (prismless) TIRFM, shown in Fig. 2B, the designed objective lens (APO 100x/1.65 N.A., oil type, Olympus) has high numerical apertures critical for proper laser alignment and specimen illumination. A filter cube composed of a 680/30 nm band-pass filter (Semrock, Inc.) was used with a CCD camera (Cascade 512B, Photometrics, Tucson, AZ, USA) with quantum efficiency identical to that of QuantEM 512SC mounted on an inverted microscope platform of an Olympus IX71. The exposure time of the CCD camera was 100 ms.

To minimize light loss, an optical mirror was used with over 90% transmission. However, the light loss occurred due to the different optical path of each TIRFM system was ignored. To reduce photobleaching, a Uniblitz mechanical shutter (Vincent Associates, Rochester, NY, USA) was used to block the 633 nm laser beam used as a light source when the camera was off. All images were collected using MetaMorph 7.1 software (Universal Imaging Co., Downing Town, PA, USA).

3. Results and discussion

3.1. Gold quenching effect on the cTnI chip

The quenching process was studied by Peteanu and required the formation of ground-state complexes between the gold and the dye-labeled DNA [19]. Also, the dominant role of the thiol group in the gold–dye interaction has been previously evaluated by performing a control experiment with a thiol-free fluorescein [20]. The magnitude of the fluorescence quenching of each dye was computed using a Stern–Volmer plot [12,21]. The ratio of the fluorescence intensity in the absence of (I_o) and in the presence of (I) the quencher is related to the concentration of the quencher ([Q]) by a coefficient K_{sv}:

$$\frac{I_o}{I} = 1 + K_{sv}[Q]$$

The photoluminescence quenching of fluorescence dyes by nano-patterned gold on the biochip also occurred. As illustrated in Fig. 3, the addition of nano-patterned gold on glass led to quenching, although the competitive optical absorption of fluorescent dye and gold on nano-patterned chip induced lower relative fluorescence intensity (RFI) compared to bare coverglass. However, the optical properties of the nano-patterned gold make them less efficient quenchers compared with gold nanospheres (GNSs) or gold nanorods (GNRs). Because GNSs and GNRs have a larger surface area and higher surface energy, they have increased numbers of quenching sites and improved quenching efficiency.

An evanescent wave was produced on either face of a sample using different optical configurations (Fig. 3). When interpreting TIRF data, it was important that the evanescent field layer intensity (I_z) decayed exponentially with increasing vertical distance (z) from the interface according to the equation,

$$I_z = I_o^{-z/d}$$

where I_o is the intensity of the evanescent field at z=0.

$$d = (\lambda/4\pi) \times \left(n_1^2 \sin^2\theta - n_2^2\right)^{-1/2}$$

The penetration depth (d), which usually ranges between 60–300 nm, was independent of the incident light polarization direction and decreased as the incident angle (θ) increased.

We controlled incident angle to same penetration depth (~113 nm) at two systems. In prism-type TIRFM, the incident angle directly measured using protractor was 67.5° (critical angle=61.2°). While the incident angles considering ultra-high N.A. (1.65) in the objective-type TIRFM system computed the corresponding penetration depth (52.02°, critical angle=48.35°) using TIRF simulator software supported in Olympus. To measure the penetration depth more correctly, we used a *z*-motor (LEP MAC 5000, LUDL Electronic Products Ltd. NY, USA).

As shown in Fig. 3A and B, when the bare coverglass was used, the RFI of the sample measured by both TIRFM systems was similar. It was supported by test using commercial nanoparticles (200 nm diameter, Molecular Probes, Eugene, OR, USA) (Fig. 4). In contrast, the RFI of sample on gold nano-patterned chip was observed

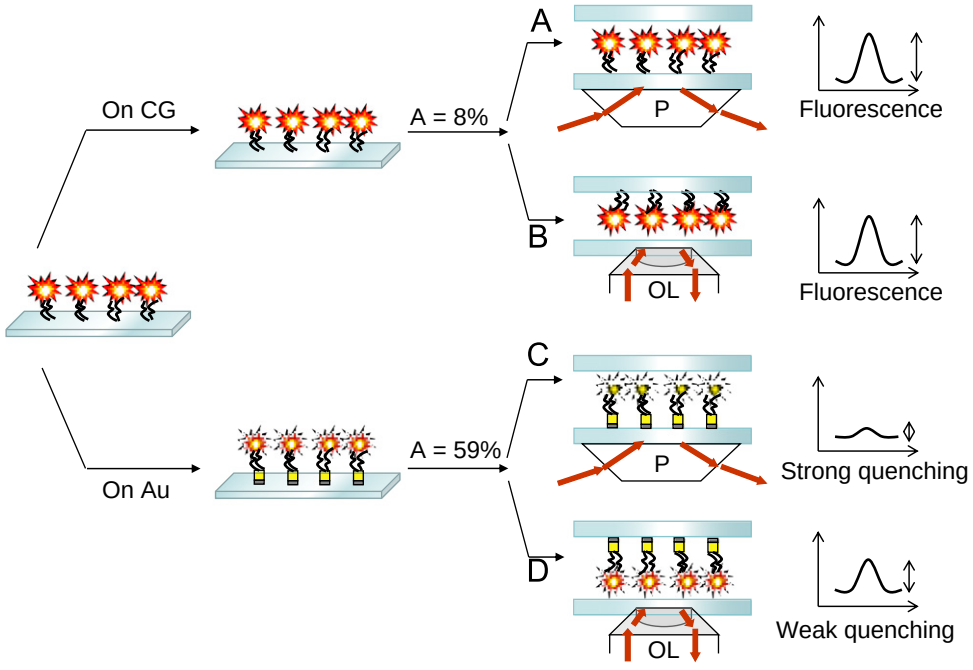

Fig. 3. The quenching efficiency of fluorescence dyes as a result of mixing the molecule and metal depended on the structure of the detection system. The following acronyms are used: CG, coverglass; Au, gold; A, absorption.

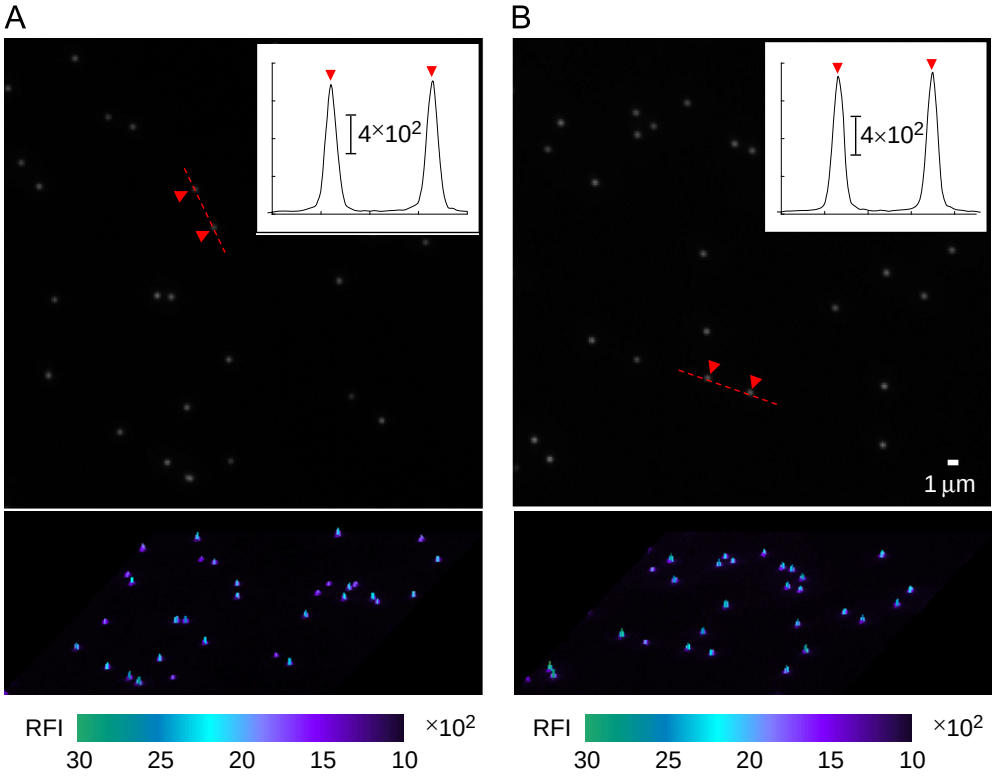

Fig. 4. TIRF image and TIR fluorescence intensity of individual 200 nm nanoparticles on bare coverglass using both TIRFM systems. (A) prism-type TRFM and (B) objective-type TIRFM.

differently because of the quenching effect (Fig. 3C and D). In the prism-type TIRFM (Fig. 3C), the laser beam illuminates the nano-patterned gold of the biochip through a prism, allowing total internal reflection to occur at the surface of the gold biochip. This indicates that the gold spot directly affects the quenching efficiency of the fluorescent dye. However, in the case of objective-type TIRFM (Fig. 3D), the laser beam was introduced into the periphery of the rear aperture of the objective. By focusing the laser beam at the rear focal plane of the objective, a parallel beam emerged from the objective lens. The angle at which the beam emerged from the objective depended on the entry position in the rear focal plane. The evanescent wave was generated at the coverglass surface, and hence the gold spot of the biochip was not an issue. Therefore, the quenching efficiency of the fluorescent dye by gold varied according to TIRFM configuration.

3.2. Detection of standard cTnI by the sandwich immunoassay

The sample chamber for antigen–antibody interaction experiments was generated by sandwiching a 1 μL volume of 1x PBS solution between a coverglass (22 mm sq) and the gold nano-patterned biochip (10 mm sq). The thickness of the solution was ~10 μm. The chip was arrayed with a 5 nm adhesive layer of chromium, followed by the deposition of a 20 nm layer of gold. The spacer arm length of DSP used as a linker for the binding of protein A/G was 1.2 nm. The protein A/G included four Fc binding domains from Protein A (5 nm) [22] and two from Protein G (1.35 nm) [23], yielding a final mass of 50.4 kDa. Generally, an IgG has substantially different orthogonal dimensions (i.e., Y-shape, height=14.5 nm, width=8.5 nm, thickness=4.0 nm) [24]. The theoretical distance of the Alexa Fluor® 647 antibody from the coverglass of the gold-patterned chip is approximately more than 71.1–74.7 nm. This indicated that the fluorescent dye (Alexa Fluor® 647) was not perfectly quenched by gold, while adsorption of dye on the metal surface resulted in the quenching of its fluorescence. Such fluorescence enhancement has been reported when the dye was located at distances greater than 10 nm from the metal surface [25,26]. Therefore, it is possible to detect the Alexa Fluor® 647 antibody, as well as to investigate the quenching effect, depending on the configuration of the system.

The quenching effect of fluorescence by gold according to the configurations of both TIRFM systems was studied by sandwich immunoassay using cTnI as a target protein. The standard curve for serially diluted standard cTnI protein is shown in Fig. 5A. The linear ranges of prism-type TIRFM (black circle) and objective-type TIRFM (white circle) were 350 pM to 84 aM (correlation coefficient, R=0.9820) and 350 pM to 35 aM (R=0.9993), respectively. High-sensitivity detection of cTnI based on the gold nano-pattern protein chip achieved a detection limit of 35 aM (S/N=3.5) with the objective-type TIRFM, which was 7000 times lower than that obtained by conventional commercial sandwich enzyme-linked immunosorbent assay (ELISA) (253 fM=6 ng/L) [27,28]. Surprisingly, the calculated relative TIRF intensities of two TIRFM types were significantly different. When the TIRF intensity of the objective-type TIRFM was referenced (100%), the measured intensity of prism-type TIRFM was 54%, 31%, 22%, 21%, and 20% with increasing cTnI concentration. Therefore, the quenching efficiency in the prism-type TIRFM was stronger than that in the objective-type TIRFM (Fig. 5B). These results are due to the different geometric structures of each TIRFM design, which determines the total internal reflection. In the prism-type system, the evanescent wave was generated at the nano-patterned gold chip (Fig. 3C), whereas the wave was generated at the coverglass surface in the objective-type TIRFM system (Fig. 3D).

Practically, nonspecific binding in cTnI sandwich immunoassay using infinitesimal concentration was ignored. The development of

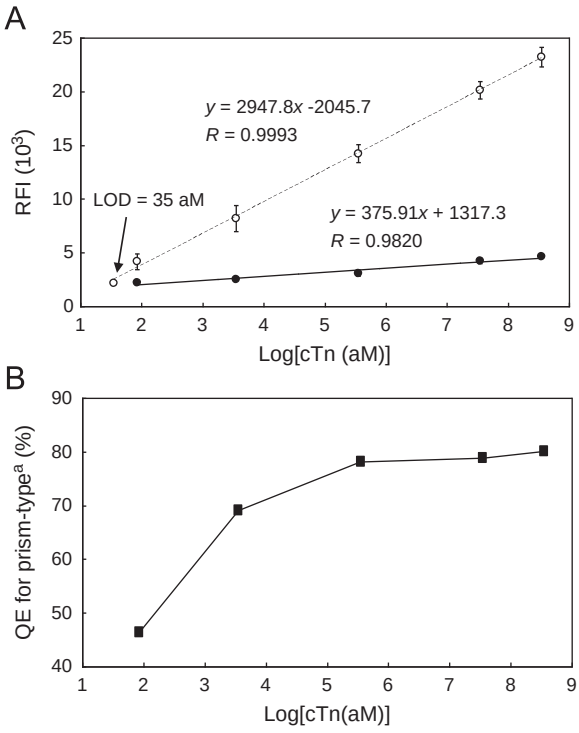

Fig. 5. (A) The calibration curve of standard troponin I concentrations produced by serial dilution, (B) quenching efficiency (QE) following calculated fluorescence intensity *via* prism-type TIRFM by increasing antigen (standard cTnI) concentration when the fluorescence intensity using an objective-type TIRFM is 100%. RFI, relative fluorescence intensity; LOD, limit of detection. Indicator: black circle, prism-type TIRF; white circle, objective-type TIRF; a, quenching efficiency of prism-type TIRF=100−(RFI in prism-type/RFI in objective-type)×100.

sandwich immunoassays for cTnI that are sufficiently sensitive to allow detection of cTnI in human serum may cause nonspecificity in distinguishing malignant and non-malignant due to moderately increased cTnI concentrations. However, since 2000; the research on monoclonal antibodies with unique specificity for individual binding sites on antigens has been suggested to improve the specificity [29,30]. Monoclonal mouse anti-cardiac troponin I antibody (clone 19C7 and 16A11) purchased from HyTest Ltd. specifically recognized the standard human cardiac troponin I (cTnI, clone 8T53). The cTnI-antibodies 19C7 and 16A11 were recommended as best pairs for quantitative sandwich immunoassay that was specific for the troponin I cardiac isoform in immunoblotting [31]. The immunological activity of antibodies was also confirmed by the producer.

3.3. Comparison of both TIRFM systems

The standard human cTnI was quantified using two TIRFM systems (prism-type *vs.* objective-type), and the significance of any difference (d_i) between the methods was determined using the paired Student's t-test. The calculated mean ($\bar{d}$) and standard deviation (S_d) of the differences were 10,647 and 6925, respectively (Table 1). The value of $t_{calculated}$ was calculated as 3.44 according to the following formula:

$$t_{calculated} = (|\bar{d}|/S_d)(n)^{1/2} = 3.44$$

where $|\bar{d}|$ is the absolute value of the mean difference.

The difference between the two assay methods was not significantly different at the 98% confidence level (t_{table}=3.747). These results showed that the signal response on the gold nano-patterned protein chip was proportional to the concentration even though there was a stronger quenching effect in prism-type system.

3.4. Clinical application of the gold nano-patterned cTnI chip

The TIRFM images of the cTnI antigen–antibody interaction on a gold nano-patterned chip are shown in Fig. 6. The individual protein molecules were attached to the gold nano-patterned surface due to efficient chemisorption of the linker to the gold surface and succinimidyl ester group. Therefore, the two types of TIRFM imaging demonstrated high signal-to-noise, though this was accompanied by a quenching effect due to the gold spot. The cTnI standard (cTnI-positive sample; Fig. 6a, 35.8 ± 5.4 fM), normal (nonpathologic) human serum (Fig. 6b, 8.9 ± 1.0 fM), and spiked human serum (Fig. 6c, 20.4 ± 4.0 fM; theoretical = 21.3 fM) were quantified using the gold nano-patterned biochip. The results indicated that the gold nano-patterned biochip assay could offer the high accuracy and sensitivity required for quantification of biomarkers in sera samples. Indeed, in the absence of a cTnI reference method and universal adoption of the National Institute on Standards and Technology (NIST) cTnI standard, it is difficult to compare absolute cTnI values. For example, the decision limit at the 99th percentile cutoff for the cTnI assay was listed as various levels from 419 fM to 20.9 pM (0.01 to 0.5 μg/L) [32,33].

Table 1
Paired *t*-test for comparing relative fluorescence intensity (RFI) differences of standard cTnI by the two methods of objective- and prism-type TIRFM.

Log[cTnI (aM)]	RFI		
	Objective-type	Prism-type	Difference
1.92	4181	2241	1940
3.54	8200	2538	5662
5.54	14,239	3112	11,127
7.54	20,148	4252	15,896
8.54	23,239	4631	18,608

Mean = 10,647; SD = 6925; $t_{calculated}$ = 3.44.

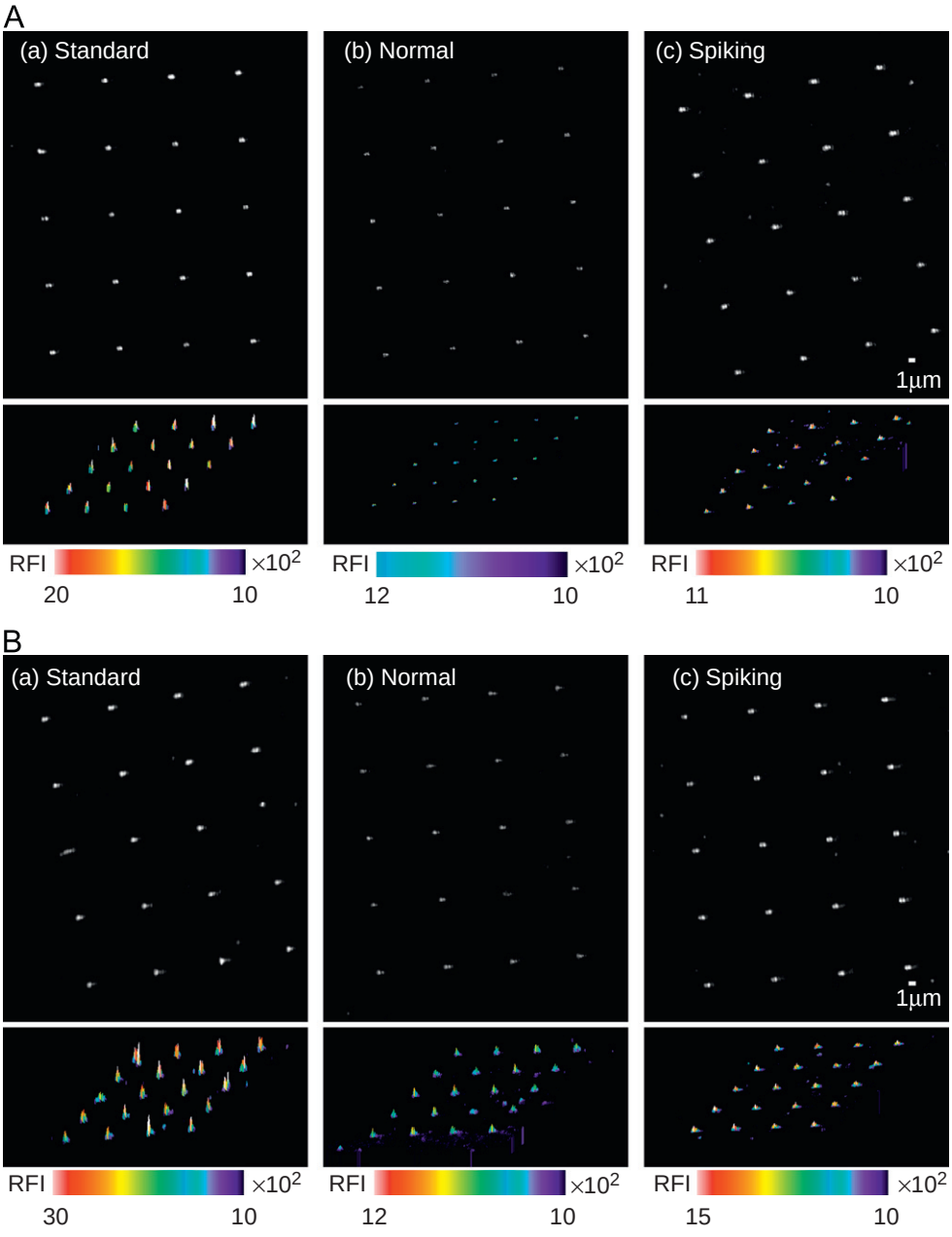

Fig. 6. (A) Prism-type and (B) objective-type TIRFM images of (a) standard cTnI (cTnI-positive sample), (b) normal (non-pathologic) human serum, and (c) cTnI-spiked human serum on gold nano-patterned biochip. The determined spot fluorescence intensities were corrected by background subtraction.

4. Conclusions

We investigated the quenching effect on a gold nano-patterned protein chip based on a sandwich immunoassay for enhanced detection sensitivity of cardiac troponin I using both types of TIRFM system. Surprisingly, the calculated relative TIRF intensities of the two types demonstrated a significant difference. The objective-type TIRFM showed higher detection sensitivity compared with that of the prism-type TIRFM. This indicates that the prism-type TIRFM experiences greater quenching efficiency by nano-patterned gold than that in the objective-type TIRFM due to the different directions of the illuminated beam created by the geometrical differences between the TIRFM systems. However, the difference between the two detection methods was not significantly different at the 98% confidence level. The results showed that the signal response on the gold nano-patterned chip was proportional to the concentration even though there was stronger quenching efficiency in the prism-type instrument.

So far, various methods such as radioimmunoassay [34] and ELISA [35–37] have been used for the direct detection of cTnI. Several manufacturers of medical diagnostics have also developed commercial immunoassay systems for the quantitation of cTnI [36]. However, troponin testing is still necessary to determine the clinical significance of low levels of troponin release with the use of high-sensitivity assays. The gold nano-patterned cTnI chip method based on the single-molecule sandwich immunoassay using TIRFM achieved improved detection sensitivity of cardiac troponin I at the aM concentration level (35 aM in objective-type and 84 aM in prism-type) and demonstrated the possibility of diagnostic application with spiked samples. Although the analytical sensitivity is capable of detection in clinical samples, nonetheless, an optimal form (more simple, faster) for point of care testing of cTnI which is important in clinical application is still awaiting in next study.

Acknowledgments

This research was supported by the Bio and Medical Technology Development Program of the National Research Foundation (NRF) funded by the Korean Government (MEST) (2012-0001130) and by Basic Science Research Program through the National Research Foundation of Korea (NRF) funded by the Ministry of Education, Science and Technology (2012R1A2A2A01013466).

References

[1] D. Axelrod, T.P. Burghardt, N.L. Thompson, Annu. Rev. Biophys. Bioeng. 13 (1984) 247.
[2] T. Funatsu, Y. Harada, M. Tokunaga, K. Saito, T. Yanagida, Nature 374 (1995) 555.
[3] X.H. Xu, E.S. Yeung, Science 275 (1997) 1106.
[4] S.H. Kang, M.R. Shortreed, E.S. Yeung, Anal. Chem. 73 (2001) 1091.
[5] K. Lee, S. Lee, H. Yu, S.H. Kang, J. Nanosci. Nanotechnol. 10 (2010) 3228.
[6] M. Tokunaga, K. Kitamura, K. Saito, A.H. Iwane, T. Yanagida, Biochem. Biophys. Res. Commun. 235 (1997) 47.
[7] K. Kitamura, M. Tokunaga, A.H. Iwane, T. Yanagida, Nature 397 (1999) 129.
[8] S. Lee, S.H. Kang, Biosen. Bioelectron. 31 (2012) 393.
[9] Olympus, 〈http://www.olympus-biosystems.com〉.
[10] Carl Zeiss, 〈http://www.zeiss.com〉.
[11] J. Malicka, I. Gryczynski, J. Fang, J. Kusba, J.R. Lakowicz, Anal. Biochem. 315 (2003) 160.
[12] B. Nikoobakht, C. Burda, M. Braun, M. Hun, M.A. El-Sayed, Photochem. Photobiol. 75 (2002) 591.
[13] R.R. Chance, A. Prock, R. Silbey, Adv. Chem. Phys. 37 (1978) 1.
[14] S.K. Ghosh, A. Pal, S. Kundu, S. Nath, T. Pal, Chem. Phys. Lett. 395 (2004) 366.
[15] E. Dulkeith, A.C. Morteani, T. Niedereichholz, T.A. Klar, J. Feldmann, M. Moller, D.I. Gittins, Phys. Rev. Lett. 89 (2002) 203002/1–203002/4.
[16] I.A. Hemmila (Ed.), Wiley, New York, 1991.
[17] M. Lee, S. Lee, J.H. Lee, H.W. Lim, G.H. Seong, E.K. Lee, S.I. Chang, C.H. Ohe, J. Choo, Biosen. Bioelectron. 26 (2011) 2135.
[18] G. Casals, X. Filella, J.L. Bedini, Clin. Biochem. 40 (2007) 1406.
[19] S. Chowdhury, Z. Wu, A. Jaquins-Gerstl, S. Liu, A. Dembska, B.A. Armitage, R. Jin, L.A. Peteanu, J. Phys. Chem. C 115 (2011) 20105.
[20] F. Cannone, G. Chirico, A.R. Bizzarri, S. Cannistraro, J. Phys. Chem. B 110 (2006) 16491.
[21] P.P.H. Cheng, D. Silvester, G. Wang, G. Kalyuzhny, A. Douglas, R.W. Murray, J. Phys. Chem. B 110 (2006) 4637.
[22] I. Bjork, Eur. J. Biochem. 29 (1972) 579.
[23] J.M. Lee, H.K. Park, Y. Jung, J.K. Kim, S.O. Jung, B.H. Chung, Anal. Chem. 79 (2007) 2680.
[24] M. Lynch, C. Mosher, J. Huff, S. Nettikadan, J. Johnson, E. Henderson, Proteomics 4 (2004) 1695.
[25] F. Stefani, G. Gerbeth, Phys. Rev. Lett. 94 (2005) 023005/1–023005/4.
[26] J.R. Lakowicz, J. Malicka, S. D'Auria, I. Gryczynski, Anal. Biochem. 320 (2003) 13.
[27] P. Venge, S. James, L. Jansson, B. Lindahl, Clin. Chem. 55 (2009) 109.
[28] C. Prontera, A. Fortunato, S. Storti, A. Mercuri, C. Boni, G.C. Zucchelli, M. Emdin, A. Clerico, Immuno. Anal. Biol. Spe. 23 (2008) 311.
[29] Z. Bian, D. Yang, C. Gu, J. Xu, G. Yang, J. Zhang, Linchuang Jianyan Zazhi 22 (2004) 9.
[30] X. Ma, X. Liu, X. Zhang, X. Hu, X. Jiang, Harbin Yike Daxue Xuebao 42 (2008) 258.
[31] 〈www.hytest.fi〉.
[32] F.S. Apple, A.H.B. Wu, A.S. Jaffe, Am. Heart J. 144 (2002) 981.
[33] A. Clerico, A. Giannoni, C. Prontera, S. Giovannini, Adv. Clin. Chem. 49 (2009) 1.
[34] B. Cummins, M.L. Auckland, R. Cummins, Am. Heart. J. 113 (1987) 1333.
[35] C. Heeschen, B.U. Goldmann, L. Langenbrink, G. Matschuck, C.W. Hamm, Clin. Chem. 45 (1999) 1789.
[36] C. Larue, C. Calzolari, J.P. Bertinchant, F. Lectercq, R. Grolleau, B. Pau, Clin. Chem. 39 (1993) 972.
[37] G.S. Bodor, S. Porter, Y. Landt, J.H. Ladenson, Clin. Chem. 38 (1992) 2203.